Available online at www.sciencedirect.com
SCIENCE DIRECT®
Geochimica et Cosmochimica Acta 70 (2006) 3275–3289
Geochimica
www.elsevier.com/locate/gca

Paleo-ocean chemistry records in marine opal: Implications for fluxes of trace elements, cosmogenic nuclides (^{10}Be and ^{26}Al), and biological productivity

D. Lal [a,*], C. Charles [a], L. Vacher [a], J.N. Goswami [b], A.J.T. Jull [c], L. McHargue [c], R.C. Finkel [d]

[a] *Scripps Institution of Oceanography, Geosciences Res. Div., La Jolla, CA 92093-0244, USA*
[b] *Physical Research Laboratory, Navrangpura, Ahmedabad 380 009, India*
[c] *University of Arizona, NSF Arizona AMS Laboratory, Tucson, AZ 85721, USA*
[d] *Lawrence Livermore National Laboratory, MS L-219, Livermore, CA 94550, USA*

Received 5 July 2005; accepted in revised form 3 April 2006

Abstract

Here, we provide evidence suggesting that marine (diatom) opal contains not only a high fidelity record of dissolved oceanic concentrations of cosmic ray-produced radionuclides, ^{10}Be and ^{26}Al, but also a record of temporal variations in a large number of trace elements such as Ti, Fe, Zn and Mn. This finding is derived from measurements in purified biogenic opal that can be separated from detrital materials using a newly developed technique based on surface charge characteristics. Initial results from a sediment core taken near the present-day position of the Antarctic Polar Front (ODP Site 1093) show dramatic changes in the intrinsic concentrations of, Be, Al, Ti, Fe, Mn and Zn in the opal assemblages during the past ~140 kyr BP. The results imply appreciable climatically controlled fluctuations in the level of bioreactive trace elements. The time series of total Be, Al, Ti, Fe and ^{10}Be in the sediment core are all well correlated with each other and with dust records in the polar ice cores. The observations suggest that a significant flux of these trace metals to oceans is contributed by the aeolian dust, in this case, presumably from the Patagonia. This observation also allows determination of fluxes of dust-contributed ^{10}Be to the Antarctica ice sheets. However, our data show that the relationships among the various metals are not perfectly linear. During periods of higher dissolved concentrations of trace elements (indicated by Fe and Ti) the relative concentrations of bioreactive elements, Be, Al, Mn and Zn are decreased. By contrast, the Fe/Zn and Fe/Mn ratios decrease significantly during each transition from cold to warm periods. The relative behavior could be consistent with any of the following processes: (i) enhanced biological productivity due to greater supply of the bioreactive elements (e.g. Zn) during cold periods (ii) increased biological and inorganic scavenging of particle active elements (e.g. Be and Al) during early interglacial periods (iii) differential uptake/removal of the metals by the various diatom taxa whose relative productivity or growth rate changes with large scale climate. In any case, with one sedimentary phase and in single sedimentary sections, we now have the potential to compare directly a proxy for aeolian input of micronutrients (e.g. Fe or Ti), with a proxy for production (e.g. ^{26}Al/Al ratios). We expect that studies of the temporal records of trace elements and cosmogenic nuclides in contrasting regions of upwelling and productivity, which exhibit different sensitivities to global climate fluctuations and micronutrient inputs, would lead to a direct and comprehensive test of ideas such as the hypothesis of iron control of atmospheric carbon dioxide [Martin, J.H., 1990. Glacial–interglacial CO_2 change: the iron hypothesis. *Paleoceanography* **5**, 1–13]. Our present data from a single site do not show that increases in dissolved Fe concentrations, per se, were responsible for increased biological productivity. However, a much clearer picture of the effect of increased dust fluxes should emerge when we have data for trace elements and the cosmogenic nuclides, ^{10}Be and ^{26}Al from various oceanic provinces.

* Corresponding author. Fax: +1 858 822 3310.
E-mail address: dlal@ucsd.edu (D. Lal).

0016-7037/$ - see front matter © 2006 Elsevier Inc. All rights reserved.
doi:10.1016/j.gca.2006.04.004

1. Introduction

The hypothesis of Martin (Martin, 1990; Martin et al., 1990) claims that biological productivity is currently limited in the Southern Ocean by the availability of Fe. In recent years, experimental evidence has grown steadily for the hypothesis of widespread iron limitation in the modern ocean (de Baar et al., 1995; Kumar et al., 1995; Watson et al., 2000; Bigg et al., 2003; Ridgewell, 2003). Throughout the history of this scientific theme, the Quaternary ice age cycles have always been considered a stringent test of the significance of this iron limitation for the carbon cycle and perhaps, the most dramatic expression of its ultimate effect on carbon sequestration (Watson et al., 2000). The ice core evidence shows that aerosol loading of the atmosphere increased during ice ages, approximately in line with significant decreases in atmospheric carbon dioxide. Yet, despite the ice core observations, and clear evidence for iron limitation in the modern ocean, the sedimentary record of "paleoproductivity" has not as yet offered any clear picture of the possible relationship between the changes in dust flux (known to have occurred over ice age cycles, for example) and regional or global productivity, over ice age cycles. A large part of the problem is that the various marine sediment proxies for dust delivery to the ocean are not diagnostic of available micronutrients (e.g. Rea, 1994) while the various indicators of paleoproductivity often lead to conflicting conclusions for any given region (e.g. Mortlock et al., 1991; Ganeshram and Pedersen, 1998; Sigman and Boyle, 2000; Chase et al., 2003).

It is obvious that these questions must be answered either by conducting experiments in the modern oceans, or by studying how the surface ocean chemistry and biology was forced in the past in different oceanic provinces, and during different climates, with changes in the aeolian dust fluxes and the dissolved concentrations of micro-nutrients and trace elements including Fe. A global picture during different climates can highlight the interrelationships between controlling factors.

In this paper, we show that it is now feasible to construct global pictures relating micro-nutrients, trace elements and biological productivity by reading the records of dissolved trace element concentrations in biogenic marine opal. The discovery that the marine opal contains a high fidelity record of dissolved oceanic concentrations of cosmic ray-produced radionuclides, ^{10}Be and ^{26}Al, and of a large number of trace elements, Be, Al, Ti, Fe, Mn, Zn, etc. appeared after several years' research on intrinsic concentrations of trace elements in three principal marine biogenic minerals: calcite, aragonite, and opal. We found that whereas foraminifera calcite and coral aragonite do include some trace elements e.g. Be and Al at ppb levels, marine opal has much higher concentrations of Al, at levels of ~1000 ppm (Dong et al., 2001; Lal, 2002). As discussed below, we verified the unexpected result of high Al concentrations in opal in several independent ways. Subsequently, we developed efficient physical and chemical techniques to extract marine opal from large amounts of sediments and then extended our studies to measurements of a suite of trace elements in marine opal from a sediment core in the present diatomaceous ooze belt. As shown below, the cosmogenic ^{10}Be and ^{26}Al and the trace element data together unambiguously establish the fact that the measured concentrations of several elements, Be, Al, Ti, Fe, Mn, Zn, etc. (in the region of 1–>500 ppm) are a true measure of their dissolved concentrations in the opaline frustule and therefore are related to the variations in their dissolved concentrations in the sea water.

Several papers have addressed the issue of (bioreactive) trace elements which are important in biological productivity (cf. de Baar et al., 1995; Watson et al., 2000; Bigg et al., 2003). Fortunately, since several of the elements enriched by the opaline frustule include Fe, Mn and Zn which are bioreactive, these studies promise to be valuable for understanding trace element controls on biological productivity in the past, as forced by climatic changes. The fact that trace element concentrations are fairly high suggests that these studies can be carried out with small amounts of marine opal, which in turn should permit extending such investigations to sedimentary sequences that lie outside the zone of the diatomaceous ooze belt. Thus, with one sedimentary phase and in single sedimentary sections, we now have the potential to compare directly a proxy for aeolian input of micronutrients (e.g. Fe), with a proxy for production (e.g. ^{26}Al/Al ratios).

The importance of combining studies of trace elements with cosmogenic ^{10}Be and ^{26}Al cannot be overestimated. The fallout of the cosmogenic nuclides is proportional to the cosmic ray flux, which can be assumed to be a constant, to a first approximation. The fallout ratio of ^{10}Be and ^{26}Al would be expected to be much more time invariant. Particle active elements, Be and Al are good indicators of biological productivity since they are scavenged more efficiently during higher biomass in the surface ocean waters. Amongst these two elements, Al shows a much greater response to biological productivity, and has been shown to be an ideal proxy for biological productivity (Ku et al., 1995). Therefore relative temporal changes in the ^{10}Be/^{26}Al ratios, and in ^{10}Be/^{9}Be and ^{26}Al/Al ratios, should constitute an important new method for inferring changes in biological productivity.

2. Oceanographic context of samples

As a "proof of concept" study of trace element and cosmogenic nuclide changes in biogenic opal, over the last full ice age cycle, we analyzed a sedimentary sequence from the heart of the Southern Ocean diatomaceous ooze belt. The sequence is comprised of ODP Site 1093 and its companion piston core TN057-13, raised at ~49°59′S, 5°52′E, near the present-day position of the Antarctic Polar Front. In the modern ocean, this site lies directly beneath the zone of relatively low salinity and in the transition zone between high and low silica content of the surface waters (presumably an

indication of uptake by diatoms). The characteristics of the surface waters in this location during cold episodes have not been established unambiguously, but, because the region is critical for regulation of atmospheric CO_2, a great deal of previous work has been conducted on other nearby cores. Some tracers such as the isotopic composition of inorganic carbon (foraminifera) and organic carbon (bulk or "diatom-bound") suggest more nutrient rich surface ocean in this region during the ice age, closer to unmodified deep water (Shemesh et al., 1993). Other surface water tracers such as Cd/Ca in foraminifera show no change (Keigwin and Boyle, 1989), but could also be interpreted as reflecting enhanced ice age nutrients (Elderfield and Rickaby, 2000). Still other tracers such as the nitrogen isotopic composition of diatom bound organic matter suggest enhanced nutrient utilization during the ice ages, perhaps because of changes in the stratification of surface ocean just south of the Polar Front (Sigman and Boyle, 2000). Thus, there is still little consensus on the relative rates of productivity and upwelling over ice age cycles.

The chronology for the cores we analyzed comes from detailed radiocarbon analyses of the uppermost 10 m (in TN057-13) and oxygen isotopic analysis of the planktonic foraminifer Neogloboquadrina pachyderma (Hodell et al., 2002; Mortyn and Charles, 2002; Mortyn et al., 2003). A composite chronology of $\delta^{18}O$ record was compiled by splicing the piston core record with that of Site 1093. Foraminifera are fairly abundant during interglacial periods but are rare or absent in glacial-aged sediments. Thus, there are unavoidable gaps in the oxygen isotopic record, but nevertheless, the delineation of marine isotope stage boundaries through the last 140 kyr is clear.

Interglacial stages are greatly expanded between MIS 1 and 15, and, conversely, glacial stages are highly compressed. A likely explanation for this pattern is relatively high biosiliceous productivity during interglacial periods when the Polar Front is near the site (as it is today), alternating with low productivity during glacial periods when seasonal sea ice expanded northward, decreasing the season for growth (Charles et al., 1991). Changes in diatom assemblages at this site (Gersonde et al., 2003) tend to support the explanation of sea ice control on biosiliceous sediment accumulation. However, other interpretations, including changes in "sediment focusing" by bottom currents, are of course possible, and, therefore it becomes especially important to develop independent tracers for productivity that carry information on rates of removal from surface waters, as opposed to only concentration information.

All through the core, an appreciable amount of ice rafted debris is present, at concentrations of the order of 1–5%, contributed by (i) volcanic glass that was presumably rafted by sea ice, and (ii) rounded quartz grains rafted by icebergs from the Antarctic continent (Kanfoush et al., 2000).

In our study, we have included measurements of two cosmogenic radionuclides, ^{10}Be (half-life: 1.5 myr) and ^{26}Al (half-life: 0.7 myr) in opal. These nuclides are produced in the high energy spallation of atmospheric nuclei, O and Ar, respectively, principally by cosmic ray neutrons. Since the elements Be and Al are particle reactive, these nuclides have short residence times in the oceans; about 500 and <50 years, respectively. Fortunately, the dissolved concentrations of ^{10}Be and ^{26}Al have been measured at several oceanic sites (Sections 4.3 and 4.4). Since the cosmic ray production rates of the ^{10}Be and ^{26}Al are small, particularly the latter, a comparison between the observed ratios $^{10}Be/Be$ and $^{26}Al/Al$ in sea water with those in opal serve as an indicator of the purity of the opal samples from detrital matter (Section 4.1).

3. Methods

Detrital material was present in all deep sea sediment samples, and therefore, it was essential to purify the opal phase thoroughly in order to analyze intrinsic trace element and cosmogenic nuclide concentrations. In previous studies, this purification has been done by differential digestion techniques combined with density separation (e.g. Shemesh et al., 1993), but we have found that such techniques are rarely 100% efficient for the purposes of trace element measurements. Furthermore, we were concerned that aggressive chemical leaching of biogenic opal surfaces (Martin and Knauer, 1973; Ellwood and Hunter, 1999) might interfere with the true trace element signature. Accordingly, we have devised a new physical separation procedure for opal that is demonstrably efficient, yet leaves the diatom frustules intact.

The readily dispersed detrital material was first separated from the sediment by gentle vibration in a conical tube. The sample was then treated with dilute HNO_3 to dissolve any foraminifera present. A variety of organic solutions and mixtures were tried to discover those which adhere strongly to opal surfaces. The basis of this method of separating opal rests in the fact that crystal surfaces often show strong affinity for certain organic compounds—for example, diamond shows strong affinity for grease. Amongst the various organic compounds tried, we found that on shaking long chain alkanes (C_6 to C_{20}) with sediment suspended in water, diatom frustules float on the top. Kerosene contains hydrocarbons in the C_{12} to C_{15} range. It remains as our chemical of choice at this time for separating opal from sediments. This method is easily adaptable for separating opal grains from sediments with very low concentrations of opal.

Additional steps were taken to *cleanse* opal of any detrital material prior to the above "flotation" procedure. First, ultrasonic dispersion and agitation of the opal sediment in ethyl alcohol (100%) was found to remove most of the detrital material easily. It is important to note here that suspension of dry sediment in alcohol does not hydrolyze or wet detrital surfaces, and detrital material tends to separate out as small clumps at the bottom of the beaker. After agitation, opal could be easily removed from ethyl alcohol by mild agitation and circular motion. Shaking with kerosene removed any detrital material present. These cleansing steps were repeated several times. The cleansed samples were checked for presence of any detrital material under a binocular microscope. In Fig. 1, we show SEM photomicrographs of cleansed diatom samples, illustrating the high purity of the samples.

We determined that whereas opal dissolved easily in dilute hydrofluoric acid (HF) at room temperature, detrital material resisted dissolution. Therefore, finally, as an additional precaution to avoid dissolution of detrital materials in HF, we therefore used only 75% of the amount of the stoichiometric amount of HF required to dissolve opal in solution for chemical analyses. The HF solutions were centrifuged, and the clear solutions were evaporated (to remove HF), and brought into solution with ICP grade 2% HNO_3. A 1/10th part of this solution was subjected to trace element analyses using an ICP-OES. The line blanks for the nine trace elements analyzed varied between (0.01–0.2) ppm. The lowest elemental concentrations were observed for Be. The ratio of average Be concentrations to blank

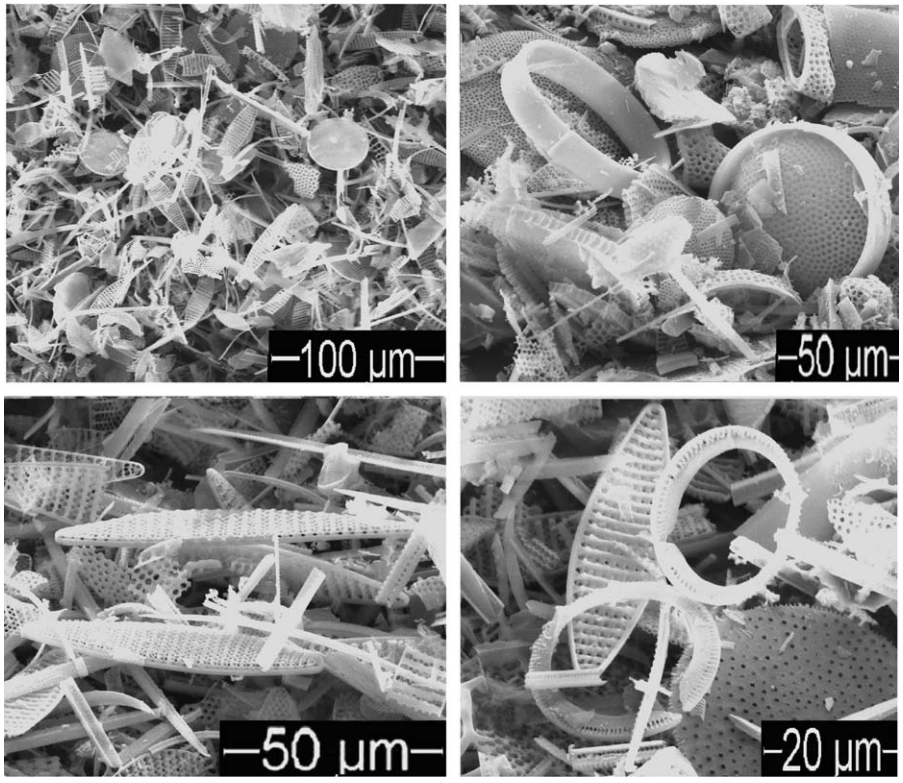

Fig. 1. Photomicrographs of diatom samples extracted using the floatation method (see text).

was ~20; for all other elements, the corresponding ratios ranged from 10^3 to 10^4. In the case of samples analyzed for ^{10}Be and ^{26}Al, about 3 mg each of ultra-pure Be and Al carriers (having ^{10}Be/B and ^{26}Al/Al ratios of $<10^{-14}$) were added. The samples were chemically processed to obtain BeO and Al_2O_3 according to standard procedures for accelerator mass spectrometry (AMS) determinations. ^{10}Be analyses were made at the AMS facility at the University of Arizona; those of ^{26}Al at the Center for Accelerator Mass Spectrometry (CMAS) at the Lawrence Livermore Radiation Laboratory, Livermore.

Independent determinations of Al and Be contents of a sample of opaline frustules were made by a Cameca ims-4f ion microprobe. Opaline frustules were pressed into a pure indium foil for analysis. A primary $^{16}O^-$ ion beam (8 nA) was used to sputter the sample and intensity of secondary ions ($^9Be^+$, $^{27}Al^+$ and $^{30}Si^+$) were measured at a mass resolving power (M/dM) of ~1400 using an electron multiplier in the pulse counting mode. GB-4 glass was used as a standard for estimating Be and Al content, assuming secondary ion yields for these elements to be similar to the GB-4 standard ($SiO_2 = 72.94\%$). Concentrations of Be and Al in the opal samples were determined using the GB-4 glass standard (Be = 11.3 ppm, Al = 8.24%; $SiO_2 = 72.94\%$) and $^{30}Si^+$ normalization. Signals from the blank (indium foil) were below detection limit for both Be and Si, while for Al a very weak signal (~0.05 cps), that is several orders of magnitude below the signal from opaline frustules, was observed.

4. Results and discussions

A total of 73 samples were analyzed from the site 1093 and its companion piston core TN057-13. In 14 of the samples, duplicate representative samples were analyzed to check on the accuracy of measurements. One standard deviation values for Be, Al, Mg, Ti, Fe, Zn, Sr and Ba were found to be 17%, 5.8%, 4.1%, 5.0%, 2.5% 4.9%, 15% and 7.7%, respectively. The high concentration levels of trace elements, ~mg/g for Al, Ca, Fe, Mg and Ti, and ~μg/g for Be, Mn, Zn and Sr, allow their easy and accurate measurements in <10 mg quantities of opal using ICP-OES. The results of trace element analyses are presented for some sections as an illustration in Table 1.

A total of 21 samples were measured for ^{10}Be concentrations. Thus far, ^{26}Al measurements were made only in five samples. These results along with the measured concentrations of Be, Al, Fe and Ti in the samples where ^{10}Be and ^{26}Al were measured, are summarized in Table 2.

4.1. Fidelity of the measurements

We must consider the question of reliability of the trace element data with respect to the possibility of contamination from detrital materials. The measured high concentrations of Al in opal (~10,000 μg/g) were unexpected (Dong et al., 2001; Lal, 2002), given that the concentration of most trace elements in the lattice structure of biogenic calcite minerals lie in the range of 1 ppb to 1 ppm. High Al concentrations of opal were previously recorded, 10–1600 μg/g (Martin and Knauer, 1973; Ellwood and Hunter, 2000), but they were considered as suspect. In any case, there are several independent tests of the fidelity of the high concentrations.

First there are general arguments based on crustal average composition (Mason, 1966). If one assumes that all of the trace element concentration arose strictly from contamination by detrital materials in the sample, one obtains a

Table 1
Measured trace element concentrations in some sections from piston cores from site 1093

Depth (m)	Age (kyr)	Element concentration (g/g)						
		Be	Al	Mg	Ti	Mn	Fe	Zn
0	0.2	3.5×10^{-7}	6.7×10^{-3}	3.3×10^{-3}	5.9×10^{-4}	1.1×10^{-3}	9.5×10^{-3}	6.8×10^{-5}
0.2	0.8	1.2×10^{-6}	3.4×10^{-3}	3.2×10^{-3}	4.7×10^{-4}	3.4×10^{-4}	7.7×10^{-3}	4.3×10^{-5}
2.1	5.5	8.1×10^{-7}	6.0×10^{-3}	3.0×10^{-3}	3.5×10^{-4}	2.1×10^{-4}	5.6×10^{-3}	4.5×10^{-5}
3	7.1	6.3×10^{-7}	4.8×10^{-3}	2.3×10^{-3}	3.0×10^{-4}	2.3×10^{-4}	4.2×10^{-3}	4.6×10^{-5}
4	8.5	5.2×10^{-7}	5.7×10^{-3}	2.6×10^{-3}	2.3×10^{-4}	1.7×10^{-4}	4.4×10^{-3}	3.6×10^{-5}
5	9.6	5.7×10^{-7}	4.0×10^{-3}	2.2×10^{-3}	2.2×10^{-4}	3.1×10^{-4}	3.7×10^{-3}	3.7×10^{-5}
6.6	11.0	1.7×10^{-7}	6.8×10^{-4}	1.8×10^{-4}	3.3×10^{-4}	3.1×10^{-4}	3.1×10^{-3}	4.2×10^{-5}
7.6	12.2	4.3×10^{-7}	3.1×10^{-4}	1.6×10^{-4}	2.0×10^{-4}	2.2×10^{-4}	3.1×10^{-3}	3.3×10^{-5}
10.08	16.4	3.8×10^{-7}	9.7×10^{-3}	3.0×10^{-5}	1.4×10^{-3}	2.0×10^{-4}	1.3×10^{-2}	7.3×10^{-5}
12.08	27.4	7.2×10^{-7}	4.3×10^{-3}	5.5×10^{-5}	9.0×10^{-4}	1.9×10^{-4}	1.2×10^{-2}	6.4×10^{-3}
13.98	42.0	8.1×10^{-7}	1.7×10^{-2}	6.5×10^{-4}	8.6×10^{-4}	2.1×10^{-4}	1.5×10^{-2}	6.0×10^{-5}
14.48	46.0	5.5×10^{-7}	8.7×10^{-3}	3.4×10^{-5}	7.0×10^{-4}	1.5×10^{-4}	1.1×10^{-2}	7.1×10^{-5}
15.58	54.3	5.0×10^{-7}	4.5×10^{-3}	1.9×10^{-5}	7.6×10^{-4}	1.6×10^{-4}	1.3×10^{-2}	4.2×10^{-3}
15.88	56.5	7.8×10^{-7}	8.7×10^{-3}	3.5×10^{-5}	8.3×10^{-4}	2.1×10^{-4}	1.4×10^{-2}	9.9×10^{-5}
17.04	64.4	7.9×10^{-7}	1.5×10^{-2}	7.8×10^{-3}	1.2×10^{-2}	2.1×10^{-4}	1.5×10^{-2}	8.9×10^{-5}
18.04	70.8	3.8×10^{-7}	2.2×10^{-3}	4.7×10^{-5}	3.0×10^{-4}	6.1×10^{-5}	4.5×10^{-3}	3.5×10^{-5}
18.74	74.6	4.0×10^{-7}	1.1×10^{-2}	3.7×10^{-3}	4.2×10^{-4}	1.6×10^{-4}	7.4×10^{-3}	4.3×10^{-3}
20.14	80.2	3.4×10^{-7}	6.8×10^{-3}	2.8×10^{-3}	3.0×10^{-4}	1.7×10^{-4}	5.0×10^{-3}	3.6×10^{-5}
20.44	81.3	4.1×10^{-7}	6.9×10^{-3}	2.9×10^{-3}	2.8×10^{-4}	1.8×10^{-4}	4.9×10^{-3}	3.9×10^{-5}
21.14	83.7	2.2×10^{-7}	9.0×10^{-4}	3.8×10^{-5}	4.0×10^{-4}	2.0×10^{-4}	3.7×10^{-3}	4.0×10^{-5}
22.14	87.2	4.9×10^{-7}	1.4×10^{-3}	3.8×10^{-5}	3.4×10^{-4}	6.3×10^{-5}	5.0×10^{-3}	3.0×10^{-5}
23.08	91.1	5.7×10^{-7}	2.5×10^{-3}	4.6×10^{-5}	6.3×10^{-4}	1.3×10^{-4}	7.0×10^{-3}	6.1×10^{-5}
23.78	94.4	4.3×10^{-7}	7.2×10^{-3}	1.2×10^{-3}	4.1×10^{-4}	1.1×10^{-4}	5.5×10^{-3}	3.0×10^{-5}
24.08	95.9	5.4×10^{-7}	9.9×10^{-3}	2.8×10^{-3}	3.9×10^{-4}	1.2×10^{-4}	5.6×10^{-3}	4.0×10^{-5}
25.88	104.6	4.3×10^{-7}	7.1×10^{-3}	2.6×10^{-3}	2.6×10^{-4}	1.3×10^{-4}	4.7×10^{-3}	2.6×10^{-5}
27.48	111.0	6.2×10^{-7}	7.8×10^{-3}	2.2×10^{-3}	2.9×10^{-4}	1.2×10^{-4}	5.9×10^{-3}	2.8×10^{-5}
28.68	114.3	4.1×10^{-7}	9.8×10^{-3}	3.2×10^{-3}	4.5×10^{-4}	1.0×10^{-4}	6.6×10^{-3}	4.7×10^{-5}
29.14	115.2	4.7×10^{-7}	1.0×10^{-2}	3.5×10^{-3}	4.2×10^{-4}	9.7×10^{-5}	6.7×10^{-3}	3.4×10^{-3}
29.54	116.1	5.8×10^{-7}	1.2×10^{-3}	2.7×10^{-3}	6.8×10^{-4}	1.8×10^{-4}	9.2×10^{-3}	6.4×10^{-5}
30.34	118.3	4.5×10^{-7}	9.3×10^{-3}	2.5×10^{-3}	6.2×10^{-4}	1.9×10^{-4}	8.3×10^{-3}	5.5×10^{-5}
31.24	121.1	4.2×10^{-7}	6.5×10^{-3}	6.6×10^{-4}	7.9×10^{-4}	3.1×10^{-4}	1.0×10^{-2}	6.9×10^{-3}
31.54	122.0	3.1×10^{-7}	4.3×10^{-3}	8.9×10^{-4}	7.0×10^{-4}	3.7×10^{-4}	8.9×10^{-3}	6.6×10^{-5}
32.14	123.9	3.6×10^{-7}	5.1×10^{-3}	3.2×10^{-3}	4.6×10^{-4}	3.5×10^{-4}	6.9×10^{-3}	5.5×10^{-5}
32.64	125.4	2.1×10^{-7}	3.5×10^{-3}	2.2×10^{-3}	2.7×10^{-4}	2.0×10^{-4}	4.0×10^{-3}	4.0×10^{-5}
33.64	128.5	1.3×10^{-7}	2.3×10^{-3}	2.7×10^{-3}	3.9×10^{-4}	8.9×10^{-4}	5.5×10^{-3}	4.7×10^{-3}
33.84	129.2	2.7×10^{-7}	3.5×10^{-3}	1.1×10^{-3}	5.4×10^{-4}	5.3×10^{-4}	8.9×10^{-3}	5.7×10^{-5}
34.44	131.6	5.5×10^{-7}	1.0×10^{-2}	2.4×10^{-3}	7.8×10^{-4}	1.5×10^{-4}	1.3×10^{-2}	6.7×10^{-5}
35.58	136.6	4.9×10^{-7}	8.2×10^{-3}	6.1×10^{-5}	1.2×10^{-3}	2.0×10^{-4}	1.2×10^{-2}	7.7×10^{-3}
35.78	137.5	5.7×10^{-7}	9.7×10^{-3}	2.7×10^{-4}	1.2×10^{-3}	1.7×10^{-4}	1.1×10^{-2}	7.1×10^{-5}

range of 8–60% for the amount of detrital material in the sample, which is most unrealistic (16.2% (Be); 9% (Al); 8.3% (Mg); 15.8% (Ca), 11.7% (Ti); 21.4% (Mn); 14.2% (Fe); 66.4% (Zn); 13% (Sr) and 60.2% (Ba)). Therefore, if the detrital contaminants are even crudely represented by bulk crustal average concentrations, these estimates rule out any significant contributions to trace element concentrations from detrital phases.

We also examined several samples of opal under the SEM for the presence of Fe or Mn coatings. EDS spot analyses and chemical maps did not reveal the presence of any appreciable concentrations of Fe or Mn or Al, which would suggest the occurrence of coatings on the particles. Similarly, from chemical and microprobe analysis, Dixit and Van Cappellen (2002) concluded that the diatom samples from the Indian sector in the Southern Ocean did not show any evidence for coatings on the diatom surfaces.

In order to check on the possibility of detrital contributions in our samples, we studied the spatial distribution of concentrations of Be and Al in a opal sample (from the Ocean Drilling Program, Leg 177, Hole 1091A (47°5.681′S, 5°55.120′E), water depth 4360.5 mbs, from the Holocene section of the core), using a Cameca ion probe (Section 3). The estimated concentrations of Be and Al in the opal sample ranged from 115 to 165 ppb, and from 560 to 1240 ppm respectively, in multiple micro-area aliquots of several samples. These concentrations agree well with the measured Be and Al concentrations in the sample using ICP (OES), 154 and 860 ppm for Be and Al respectively (Dong et al., 2001).

A third test involves the $^{26}Al/Al$ ratio of the purified opal. The dissolved concentrations of ^{26}Al and Al have been measured by Ku et al. (1995) in two locations in the eastern Pacific Ocean at 12°N, 140°W and 12°N, 135°W. The measured ratios, $^{26}Al/Al$ were found to be

Table 2
Measured ^{10}Be and ^{26}Al concentrations in marine opal samples from site 1093

Depth (m)	Age (kyr)	^{10}Be concentration (atoms/g)	Intrinsic ratio (^{10}Be/^{9}Be)	^{26}Al concentration (atoms/g)	Intrinsic ratio (^{26}Al/Al)
1.14	5.82	$(1.8 \pm 0.002) \times 10^{9}$	$(5.4 \pm 0.04) \times 10^{-8}$	$(4.4 \pm 1.1) \times 10^{6}$	$(1.4 \pm 0.4) \times 10^{-14}$
5.60	10.18	$(1.9 \pm 0.007) \times 10^{7}$	$(2.0 \pm 0.01) \times 10^{-7}$	na	na
8.58	13.69	$(1.7 \pm 0.07) \times 10^{5}$	$(1.9 \pm 0.07) \times 10^{-9}$	na	na
10.48	18.24	$(1.8 \pm 0.07) \times 10^{7}$	$(4.3 \pm 0.2) \times 10^{-8}$	na	na
12.08	27.38	$(5.6 \pm 0.02) \times 10^{7}$	$(1.2 \pm 0.01) \times 10^{-7}$	na	na
12.68	31.78	$(4.0 \pm 0.009) \times 10^{7}$	$(6.4 \pm 0.01) \times 10^{-8}$	na	na
12.98	34.08	na	na	$(1.8 \pm 1.5) \times 10^{6}$	$(1.8 \pm 3.0) \times 10^{-15}$
13.98	42.01	$(3.1 \pm 0.008) \times 10^{7}$	$(5.8 \pm 0.01) \times 10^{-8}$	na	na
14.48	45.97	$(2.4 \pm 0.006) \times 10^{7}$	$(6.7 \pm 0.02) \times 10^{-8}$	na	na
15.28	52.1	$(3.1 \pm 0.01) \times 10^{7}$	$(5.0 \pm 0.02) \times 10^{-7}$	na	na
15.88	56.5	$(2.0 \pm 0.005) \times 10^{7}$	$(3.9 \pm 0.01) \times 10^{-8}$	na	na
17.04	64.35	$(5.0 \pm 0.01) \times 10^{7}$	$(9.4 \pm 0.02) \times 10^{-8}$	na	na
18.04	70.78	$(2.2 \pm 0.006) \times 10^{7}$	$(8.7 \pm 0.02) \times 10^{-8}$	na	na
21.44	84.79	$(3.0 \pm 0.007) \times 10^{7}$	$(6.4 \pm 0.01) \times 10^{-8}$	na	na
23.08	91.07	$(3.7 \pm 0.01) \times 10^{7}$	$(9.8 \pm 0.03) \times 10^{-8}$	na	na
24.68	98.93	$(2.4 \pm 0.007) \times 10^{7}$	$(1.7 \pm 0.01) \times 10^{-7}$	$(4.7 \pm 1.6) \times 10^{6}$	$(2.0 \pm 0.7) \times 10^{-15}$
25.13	101.22	$(1.6 \pm 0.004) \times 10^{7}$	$(1.2 \pm 0.01) \times 10^{-7}$	$(2.2 \pm 0.6) \times 10^{6}$	$(1.2 \pm 0.3) \times 10^{-14}$
26.28	106.3	$(3.4 \pm 0.009) \times 10^{7}$	$(7.6 \pm 0.02) \times 10^{-8}$	na	na
28.18	113.26	$(3.2 \pm 0.01) \times 10^{7}$	$(7.3 \pm 0.03) \times 10^{-8}$	na	na
31.24	121.09	$(3.5 \pm 0.01) \times 10^{7}$	$(1.2 \pm 0.01) \times 10^{-7}$	na	na
32.64	125.41	$(9.8 \pm 0.03) \times 10^{6}$	$(6.3 \pm 0.02) \times 10^{-8}$	na	na
34.83	133.29	na	na	$(7.1 \pm 0.6) \times 10^{5}$	$(2.5 \pm 2.2) \times 10^{-15}$

na, not available.

($<$2–18) $\times 10^{-14}$, with Al concentrations of (1–3.5) nM. The lowest ^{26}Al/Al ratios which can be measured using present generation accelerator mass spectrometers is $\sim n \times 10^{-15}$, with $n \sim 2$–5. If our Al extracts from opal included detrital Al, the ^{26}Al/Al ratios would be lowered. Let us, for the sake of argument assume that the maximum intrinsic Al concentrations in opal were only of the order of 1–10 ppm, as against the measured values of 10^{-3} to 10^{-2} g/g (Table 1), and that the measured values were due to detritus contamination, then the ^{26}Al/Al ratios would be lowered to values of 10^{-18} to 10^{-17}, two to three orders of magnitude below detection limit using the AMS. In fact the measured ^{26}Al/Al ratios (Table 2) lie in the range of (7.4×10^{-15} to 6×10^{-14}), quite consistent with the range of the observed ratios in seawater (Ku et al., 1995). In fact, any significant measurement of ^{26}Al/Al ratio in the opal in fact is a testimony to a fairly pure extraction of Al from the opaline frustule. Our data, though limited to five samples demonstrate the effectiveness of opal in picking up dissolved Al ions from seawater, and also to the fact that the aluminum extracted from the opal is fairly free from any detrital contamination.

Finally, to check on the possibility that an appreciable part of the trace elements existed as adsorbed on the outer surfaces of the opal samples, we carried out congruent dissolution of cleansed diatom samples. We carried out dissolution of about 40–60% of the opal in three samples and measured the trace element concentrations in the first and second fractions. For another three samples we made three successive dissolutions of ~20–40% of the opal in each case. The standard deviation in these experiments varied between 15% and 50%, the errors mostly arising from the errors in estimation of the fraction of sample dissolved in successive dissolutions. A part of the observed variation may be due to differences in the enrichment factors for different diatom species, which dissolved differentially during HF dissolution. The results however clearly showed that the trace elements were not preferentially adsorbed on the outer surfaces of the opaline frustules.

Our observations raise important questions: Why are the element distribution coefficients so large in opal, and where are the trace elements trapped in the opal? The current understanding of the process of silica polymerization and structure formation in the diatom cell wall (Hildebrand and Wetherbee, 2003) indicates that entrapment of metal ions within the silica structure, as opposed to external surface absorption, is very feasible. These studies show that the formation of the diatom cell wall occurs in two steps: (i) formation of the pattern of the overall two-dimensional structure, which entails formation of a thin layer of silica, and (ii) a "filling in" process, whereby the two-dimensional patterned structure is expanded in a third dimension. The substantial interstitial spaces in the polymerizing silica structure (Hildebrand and Wetherbee, 2003; Hilderbrand, priv. Communication, 2004) could easily accommodate metal ions or other molecules. Direct evidence for entrapment of molecules in diatom silica has also been demonstrated, in two ways. First, positively charged or amine-containing fluorescent dyes accumulate in the silica deposition vesicle (SDV) and become incorporated in the silica suggesting that positively charged compounds are readily accommodated in this compartment. Additionally, long-chain polyamines and amino-group rich proteins (silaffins) have been implicated in accelerating silica formation inside the SDV (Kröger et al., 1999, 2000). The amino groups of these compounds may also be able to act as

ligands for complexation of transition metal ions and thus facilitate accumulation of these ions inside the SDV. Second, fluorescent dyes have been incorporated into diatom silica (in the living organism during silica polymerization) in abundant amounts (Li et al., 1989). These dyes remain associated with the silica even after harsh acid treatment, indicating that they are incorporated throughout the material and are not exclusively associated with the surface.

The observations of Dixit and Van Cappellen (2002) showed that silanol groups on biogenic silica are excellent ligands for aluminum. These authors concluded that since biologically important trace metals such as Cd, Zn and Fe also exhibit strong affinity for silica surfaces at neutral to alkaline pH conditions (Criscenti and Sverjensky, 1999), adsorption onto diatom shells and export to deep ocean may be an important pathway for removing metals from surface ocean. Our observations based on congruent dissolution of cleansed opal samples are consistent with the inference that the trace elements were not preferentially adsorbed on the outer surfaces of the opaline frustules. This is also supported by the lack of evidence for coatings on diatom samples. We therefore conclude that trace metals are primarily distributed within the silica matrix rather being primarily adsorbed on outer surfaces on to silanol groups, as suggested by Dixit and Van Cappellen (2002).

In summary, all of our experiments strongly suggest that the measured concentrations of trace elements refer to their intrinsic concentrations in the opaline frustule and that on the average, the concentrations of the elements lie in the range of 50–7000 ppm for the elements listed in Table 1, except for Be whose average concentration is ~0.5 ppm. We would like to point out here that our results for Al and Zn are lower than those reported earlier Martin and Knauer (1973) and Ellwood and Hunter (1999). As was mentioned earlier, this discrepancy is probably a result of the fact that these authors used harsh leaching procedures using strong HNO_3 and HCl solutions to clean opal.

4.2. Trace element records over 140 kyr

In Fig. 2, we show the measured ^{18}O and concentrations of Fe, Al, Ti, Mn and Zn in the 140 kyr BP section. One observes similar excursions for Fe and Al. Data for Fe are therefore plotted separately for this reason; the five elements show similar features, with high values at 20–25, 35–65 kyr BP, and lows during 0–15, 100–110 and 125–135 kyr BP. The maxima show a general temporal correspondence with increased dust concentrations during colder periods, as recognized from observations in the GISP2 and Vostok ice cores (Jouzel et al., 1993; Mayewski et al., 1997). In GISP2, Ca concentrations have been

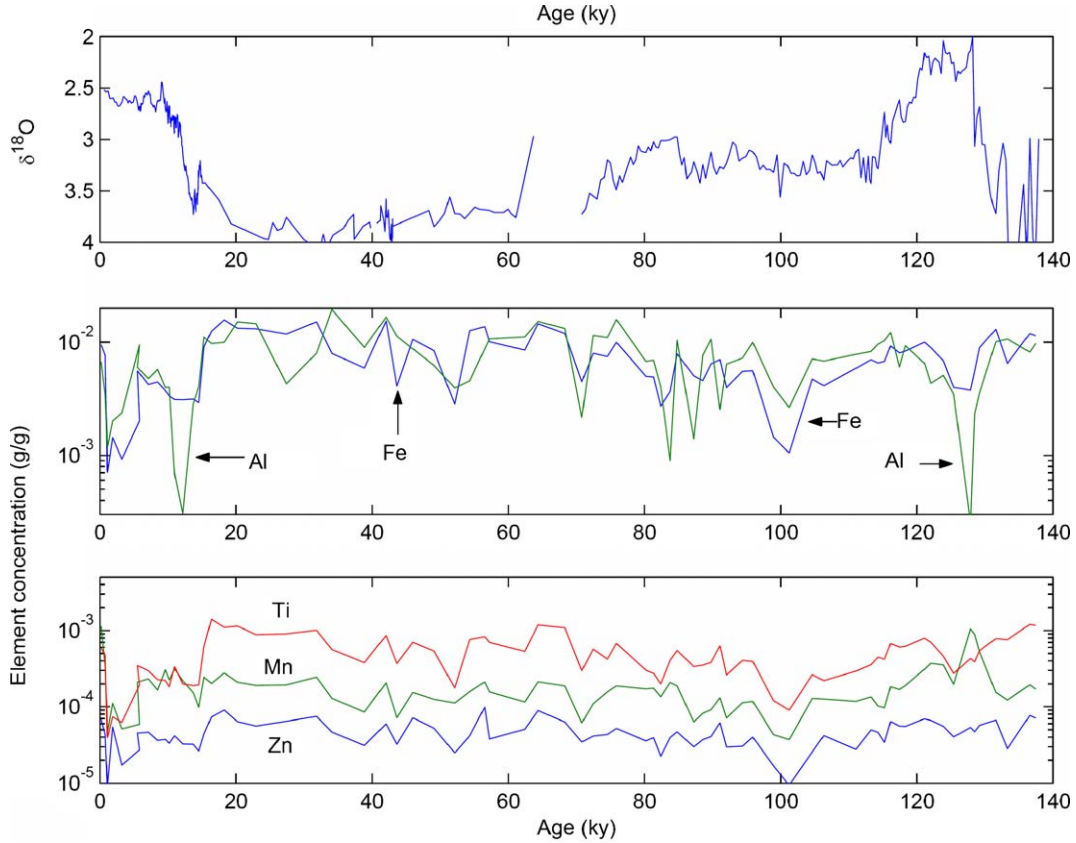

Fig. 2. Measured concentrations of Fe, Al, Ti, Mn and Zn in opal samples from a piston core from site 1093 are shown along with measured $\delta^{18}O$ values in the core.

measured (Mayewski et al., 1997), which are indicative of dust concentrations. This relationship can be clearly seen in Fig. 3, and it suggests a prominent role of winds in delivering higher fluxes of mineral aerosol to ocean surface during colder periods, causing prominent excursions in intrinsic concentrations of several elements, particularly reactive elements which have very low dissolved concentrations (a consequence of short residence times) in oceans. We must caution here however that, even if aeolian deposition in part determines the availability of elements such as Ti, Be and Al, we should not necessarily expect a linear relationship between source strength (dustiness) and the relative concentrations of bioreactive elements which are incorporated in siliceous skeletons. One possible example of the decoupling between dust and trace elements is the fact that the trace element concentrations in opal do not fall to zero in the peak interglacial periods, despite the evidence for negligible dust accumulation recorded in the contemporaneous sections of the Vostok ice core. This discrepancy could be an indication that there are other sources for the metals aside from dust—especially the upwelling of subsurface water (Measures and Vink, 2001; Latimer and Flippelli, 2001)—but it could also reflect the differential uptake and scavenging of various diatom assemblages (discussed below).

In general, it should be possible to calculate opal-derived metal fluxes to the sediment using these concentration data and the total sediment accumulation. In this sedimentary sequence, the calculated opal-derived Fe flux is approximately 1×10^{-5} g/cm^2/y. For comparison, this flux is two orders of magnitude higher than the estimated flux of iron to the surface ocean in the South Pacific (Measures and Vink, 2001). However, the significance of this comparison is questionable without a better sense of spatial variability of either the sources or sinks of the various trace elements. For example, the modern (Holocene) opal accumulation at this site ranks among the highest in the global ocean, and therefore the trace element flux calculated from these sediments cannot be extrapolated as a regional average.

In Fig. 4, we have plotted the mean residence times and elemental enrichment factors (Efs) for opal. The mean oceanic residence times and elemental concentrations are based on Riley and Chester (1981). The Efs are calculated relative to Ca, and not Si (whose dissolved concentration in surface seawater is very variable). Data in Fig. 4 show that generally elements with shorter residence times in seawater have higher enrichment factors. This may simply be a reflection of the fact that more chemically and biologically active elements (shorter residence time species) are more easily incorporated in the opaline frustule (higher enrichment factors).

4.3. Discussion of measured ^{10}Be concentrations in a 140 kyr BP section

The measured ratios of ^{10}Be/Be, ^{26}Al/Al and ^{10}Be/^{26}Al (Table 2) in the opaline frustule lie in the range of

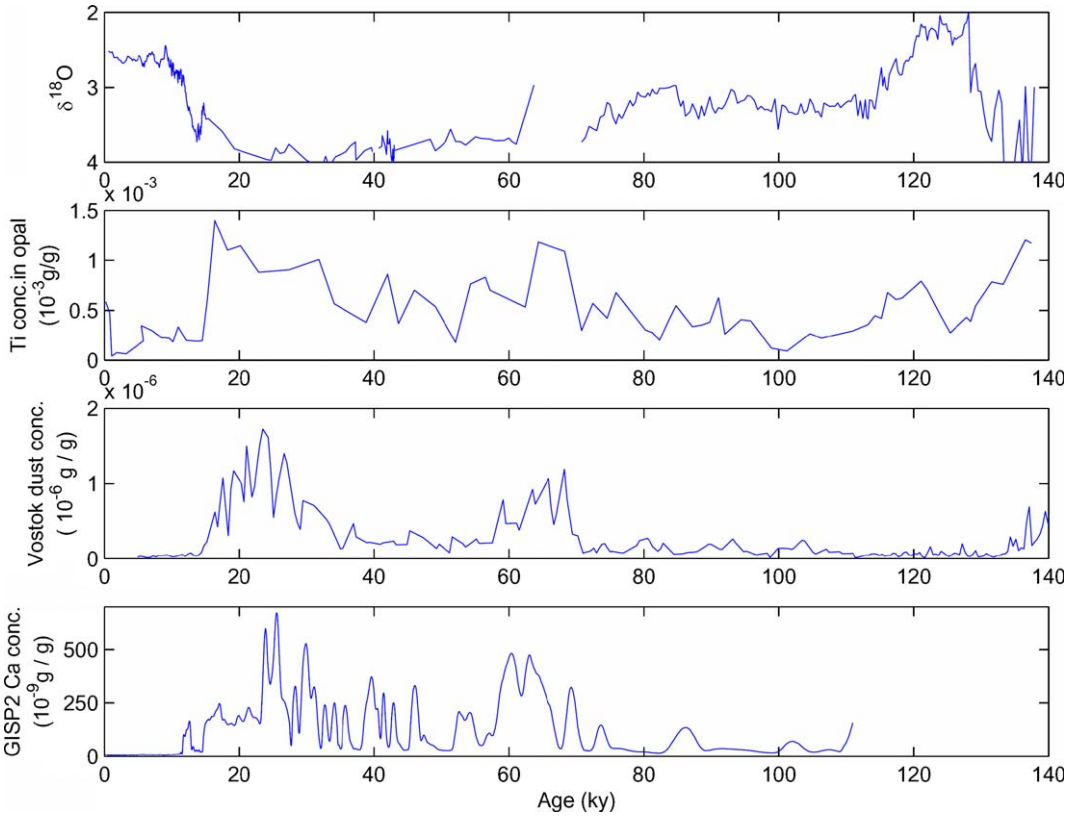

Fig. 3. Plots of measured Ca concentrations in GISP2 (Mayewski et al., 1997) and of dust concentrations in Vostok (Jouzel et al., 1993) ice cores are shown along with measured δ^{18}O values in foraminifera, and Ti concentrations in opal samples along the core from site 1093, during the past 140 kyr B.P.

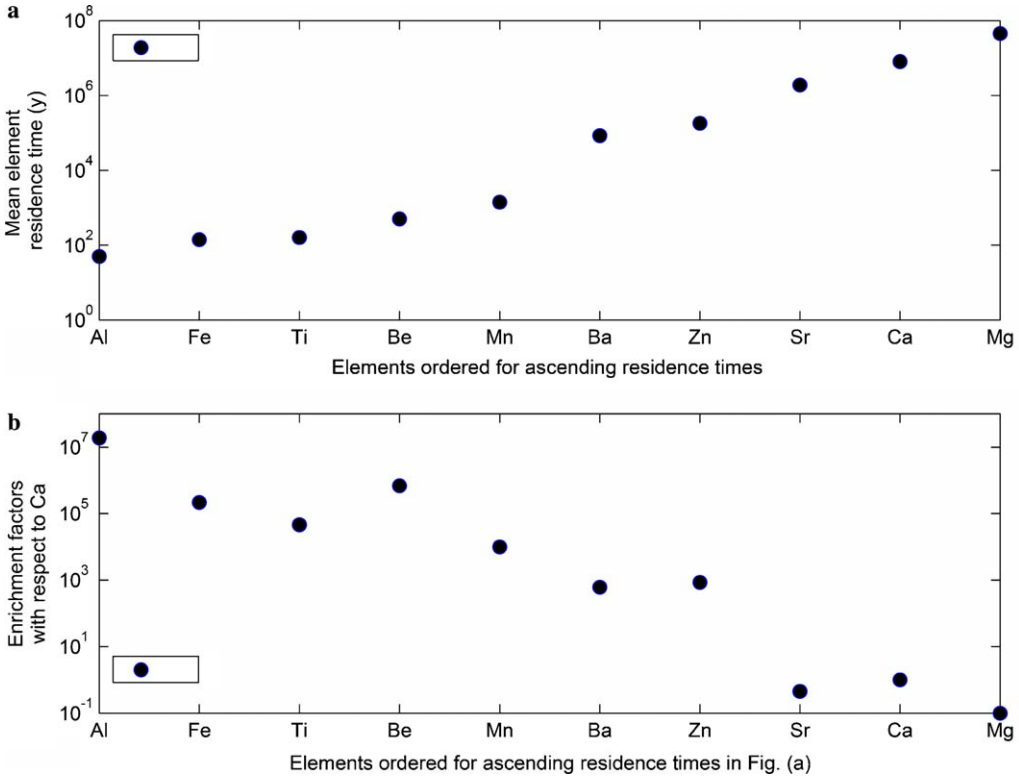

Fig. 4. The top figure is a plot of the mean oceanic residence times of elements, arranged in order of *ascending* residence times. The lower figure gives the measured enrichment factors (Efs) for opal for the elements, based on mean seawater concentrations (see text).

(5×10^{-8} to 1.7×10^{-7}), (7.4×10^{-15} to 6×10^{-14}) and (4×10^{2} to 7×10^{2}), respectively. Each of these ratios lies in the range of the observed ratios in the dissolved phases in seawater (Kusakabe et al., 1987; Ku et al., 1990, 1995; Measures et al., 1996). The agreement of these ratios with the sea water ratios demonstrate the effectiveness of opal in picking dissolved Be and Al ions from seawater, and these ratios also provide further evidence that the trace elements extracted from opal are fairly free from any detrital contamination. We would also like to note from the data in Table 2, that ^{10}Be can easily be measured in ~100 mg opal, and ^{26}Al in ~10 g opal.

Measured ^{10}Be concentrations (Table 2) show a temporal variation similar to that for trace elements in Fig. 2, suggesting a common origin for the variability. This can be seen clearly from Figs. 5 and 6. In Fig. 5, we have plotted the opaline ^{10}Be concentrations as a function of elemental concentrations for Be, Al, Ti and Fe. During periods of low concentrations of these elements, ^{10}Be concentrations are the lowest, $\sim2\times10^{9}$ atoms ^{10}Be/g opal; they increase monotonically with increasing elemental concentrations, reaching a value of $\sim4\times10^{9}$ atoms ^{10}Be/g opal. The data show a scatter of ~20%, but the data clearly point to a direct flux of ^{10}Be with aeolian dust, the minimum value of $\sim2\times10^{9}$ atoms ^{10}Be/g owing itself to the cosmic ray-produced ^{10}Be, which is added to oceans mainly by scavenging of atmospheric^{10}Be by wet precipitations, the normal mode of fall out of ^{10}Be.

Further details on the direct flux of ^{10}Be via aeolian dust is manifest from Fig. 6, where we have plotted the ^{10}Be/Be ratios in opaline frustule as a function of elemental concentrations for Be, Al, Ti and Fe. Here, we see that at low elemental concentrations, the ratios are $>10^{-7}$, with the highest value of $\sim5\times10^{-7}$. With increasing concentrations, the ratios fall asymptotically to a value of $\sim(5\text{–}6)\times10^{-8}$ in each of the element plots. These data imply that we can determine ^{10}Be/Be ratios in seawater with and without significant aeolian flux to the surface. The measured surface ^{10}Be/Be ratios in Pacific and Antarctic oceans range between $(1\text{–}3)\times10^{-7}$, the highest value of $\sim3\times10^{-7}$ being for the Antarctic surface water (Kusakabe et al., 1987; Ku et al., 1990). The high value of the Antarctic sample is interpreted by Ku et al. (1990) as due to inputs from melt waters rich in ^{10}Be.

The increase in the flux of ^{10}Be with higher aeolian fluxes is expected since the typical ^{10}Be concentrations in continental surface soils is of the order of 10^{9} ^{10}Be atoms/g, with typical ^{10}Be/Be ratios of $(0.2\text{–}1)\times10^{-7}$ (Barg et al., 1997). According to studies by Brown et al. (1992) and Measures et al. (1996), Be present in dust shows high solubility in ocean water. The ^{10}Be amount added with addition of Be from the dust, $\sim2.5\times10^{9}$ ^{10}Be atoms/μg Be as well as the plateau ratio ^{10}Be/Be value of $\sim(5\text{–}6)\times10^{-8}$ in Fig. 6 are therefore quite consistent with the continental surface soil data. It seems a fair assumption that the predominant source of dust is Patagonia (Basile et al., 1997).

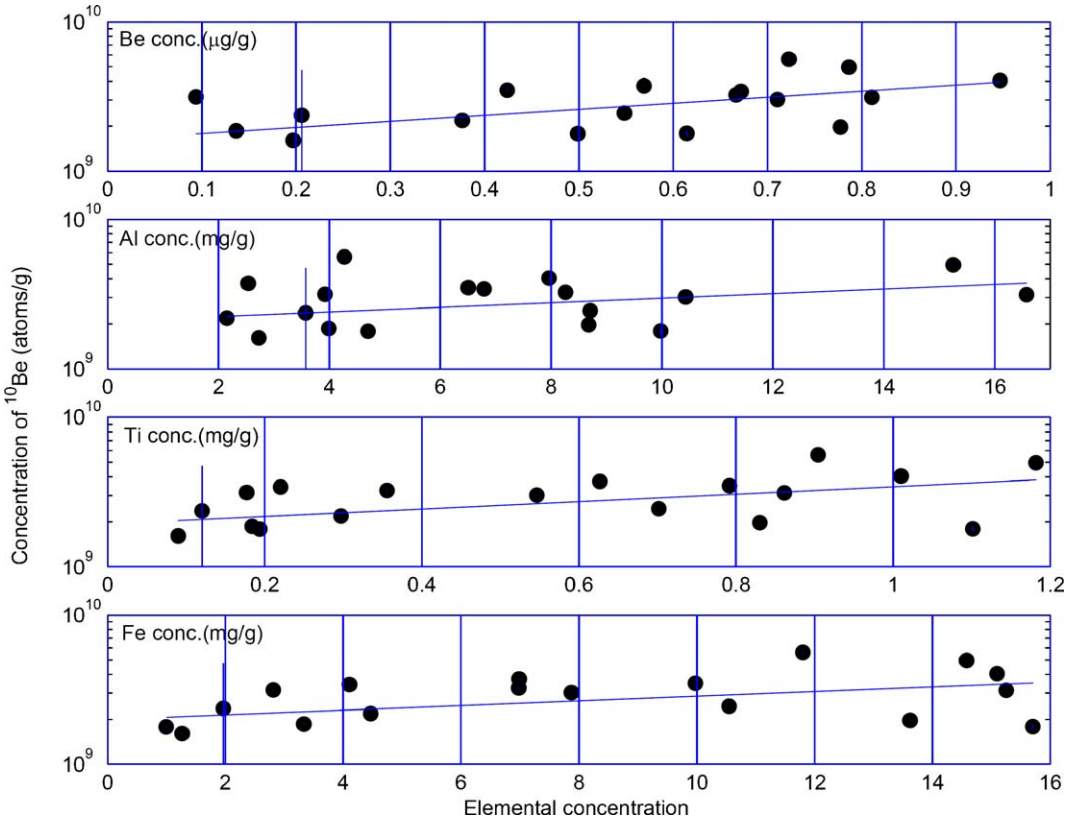

Fig. 5. Measured ^{10}Be concentrations in opal in the 140 kyr section from site 1093 are plotted versus concentrations of Be, Al, Ti and Fe. The best fit lines are power-law fits.

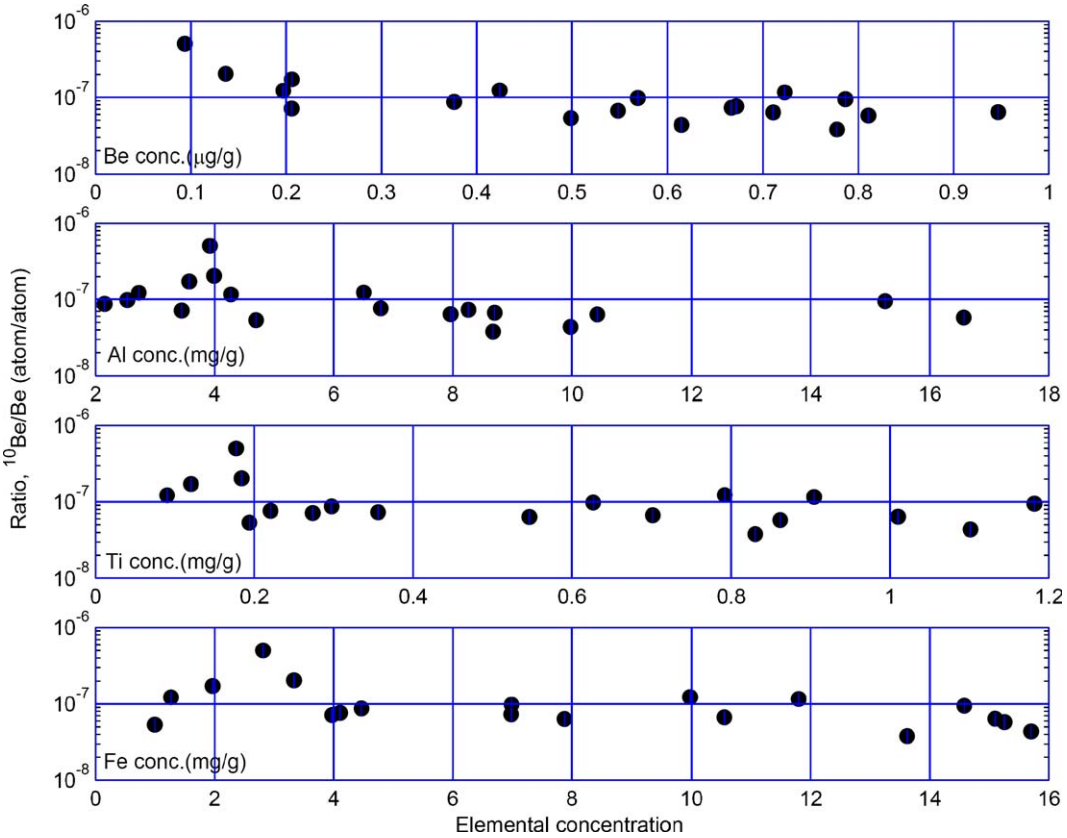

Fig. 6. Measured ^{10}Be/Be ratios in opal in the 140 kyr section from site 1093 are plotted versus concentrations of Be, Al, Ti and Fe.

Finally, one notes in Figs. 5 and 6 that the behavior of ^{10}Be concentrations and ^{10}Be/Be ratios shows significant differences with the element considered, particularly in the case of Al.

4.4. Measured ^{26}Al concentrations in relation to aeolian fluxes

Our data on ^{26}Al are, as yet limited to five samples. In Fig. 7, we have plotted measured ^{26}Al concentrations in opaline frustules as a function of concentrations of Be, Al and Fe. Similar behavior is seen for a plot of ^{26}Al/Al ratio vs. Al. The decrease in ^{26}Al concentrations with increasing elemental concentrations would be expected through either increased scavenging or increased biological productivity, or through the addition of Al from dissolution of aeolian dust. Considering the latter possibility, ^{26}Al concentrations of soils are expected to be lower by a factor of >300 (Lal and Peters, 1967) than of ^{10}Be because of its lower production rate, leading to an expectation of $<3\times10^{6}$ atoms ^{26}Al/g soil. The ratio ^{26}Al/Al in soils is expected to be $<1\times10^{-14}$. The absolute concentration and the ratio in soils are both comparable to the values measured in opal. Care has therefore to be taken in interpreting the ^{26}Al data. It is however clear that the most interesting part of the ^{26}Al data would be both the low and the high end of the elemental concentrations in Fig. 7. Our data are limited but we see that at low Al concentrations, <5 mg/g opal, both high and low ^{26}Al/Al ratios are observed. Within the errors of measurements, the lowest ratio, $\sim0.7\times10^{-14}$ is similar to the value at high Al concentrations, $\sim0.5\times10^{-14}$. The latter ratio is probably determined primarily by the dilution effect due to addition of soil ^{26}Al and Al in the ocean water, but the former by biological productivity!

The principal reason to include ^{26}Al and ^{10}Be in the analyses is to separate the two effects of input and uptake, which should be possible since Al shows a much greater response to biological productivity than Be, and is considered therefore to be an ideal proxy for biological productivity (Ku et al., 1995).

5. Control of Fe concentrations on biological productivity

There are two avenues available to us for examining the role played by Fe in affecting biological productivity as a function of increased inputs of Fe to the oceans, by examining: (i) interrelationships between Fe and Ti as a function of variations in the concentrations of other bioreactive elements, and (ii) how the absolute concentration of ^{26}Al change with increased flux of Fe to the surface. Increased dust fluxes of which Ti is a good indicator, increases the oceanic fluxes of the cosmogenic nuclides, ^{10}Be and ^{26}Al, as discussed above, but in a known fashion. The short

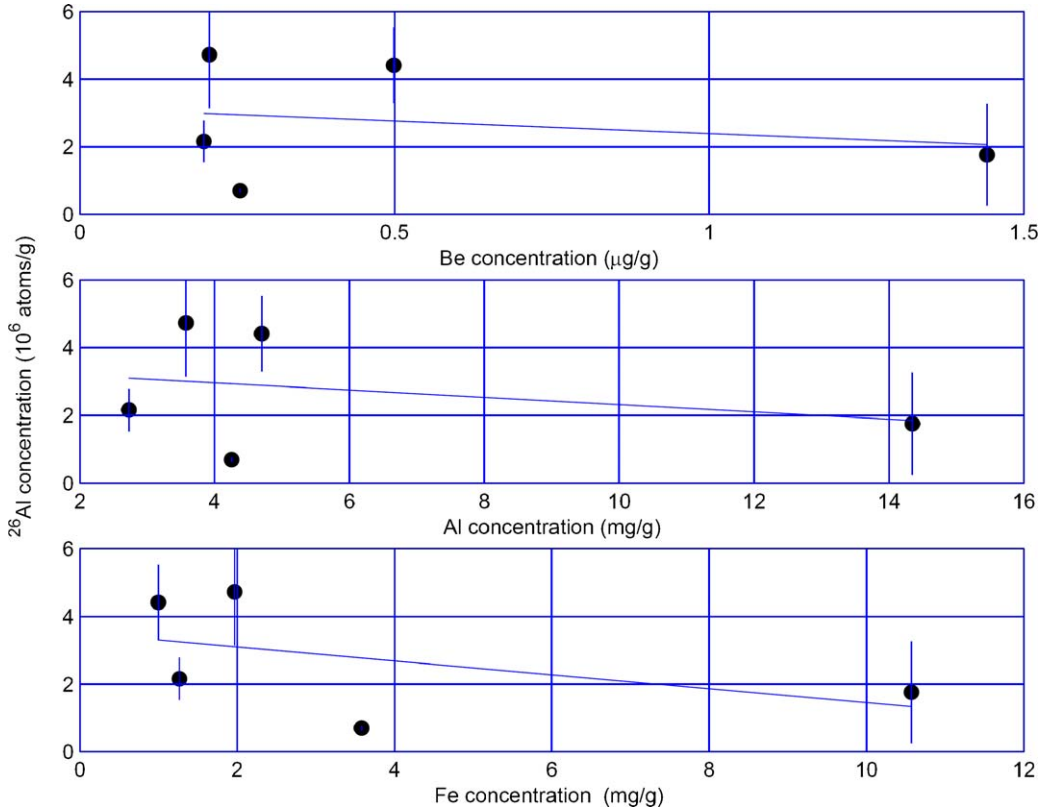

Fig. 7. Measured ^{26}Al concentrations in opal in the 140 kyr section from site 1093 are plotted versus concentrations of Be, Al and Fe. The best fit lines are power-law fits.

residence time of dissolved Al (dominantly controlled by biological uptake) compared to Be in the oceans forms a good handle to separately evaluate the roles of particle scavenging and biological uptake. A set of equations can be set up to see how the trace element concentrations are affected by particle scavenging and biological uptake, with normalization with $^{26}Al/Al$ ratios. However, since our ^{26}Al data are very limited, we will only examine the relationships between concentrations of different elements in opal samples as a function of concentration of Fe.

The variation of ratios of concentrations of Fe with different elements, Be, Al, Ti, Mn and Zn, Fe is shown in Fig. 8, as a function of Fe concentration, which varies by more than one order of magnitude in the samples. Trends are clearly seen in spite of the scatter in the data. The smallest slope is seen in the case of Ti, consistent with a constant Fe/Ti ratio of ~15, which just shows that increase in the dissolved concentrations of Fe and Ti keep in step. The similarity between the Ti and Fe suggests that dust input controls the temporal variability of both elements, despite the fact that the upwelling of subsurface waters may supply the dominant fraction of Fe to the surface waters in the present ocean (Measures and Vink, 2001), The three bioreactive elements, Al, Zn and Mn, on the other hand, show a significant and similar positive slope, corresponding to an increase in the Fe/element ratio by a factor of about 5 for a 20-fold increase in Fe concentration.

This behavior could indicate that two principal processes become operative with increased aeolian fluxes (as indicated by increase in the dissolved fluxes of Fe and Ti): (i) increased biological productivity resulting from greater availability of bioreactive elements, and (ii) increased biological and inorganic scavenging of particle active elements. If this hypothesis is valid, and because Ti has so far not been indicated in any of the studies to affect or to control biological productivity, these results would imply that the accompanying increase in the concentration of bioreactive trace elements, not Fe, was responsible for increased biological productivity. Of course, even so, we could not rule out the possibility that in Fe deficient waters, addition of small amounts of Fe initially makes a large difference in the biological production.

However, another way of viewing the metal results is to plot the time series of the concentration ratios (Fig. 9). From these various trends, it is clear that, for each of the metal ratio pairs, there is a repeated relationship to (orbital scale) climate change. It is also clear that the behavior of Be and Al is distinct from that of Zn and Mn—an important observation, given that Zn and Mn are the elements known to be essential for diatom growth. In any case, Fe/Be or Fe/Al ratios follow a broad glacial-interglacial fluctuation, with minima during the late interglacial periods. On the other hand, Fe/Zn and Fe/Mn ratios display a consistent pattern of excursion to low values during the major

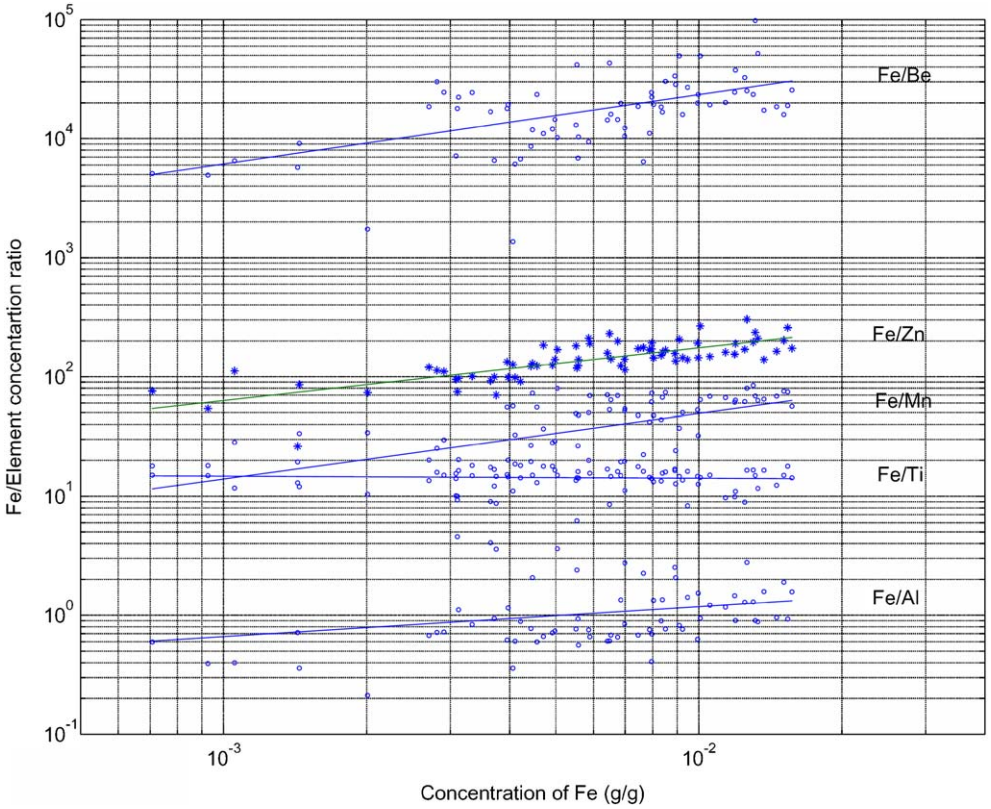

Fig. 8. The ratios of Fe/element concentrations in opal in the 140 kyr section from site 1093 are plotted different as a function of concentration of Fe.

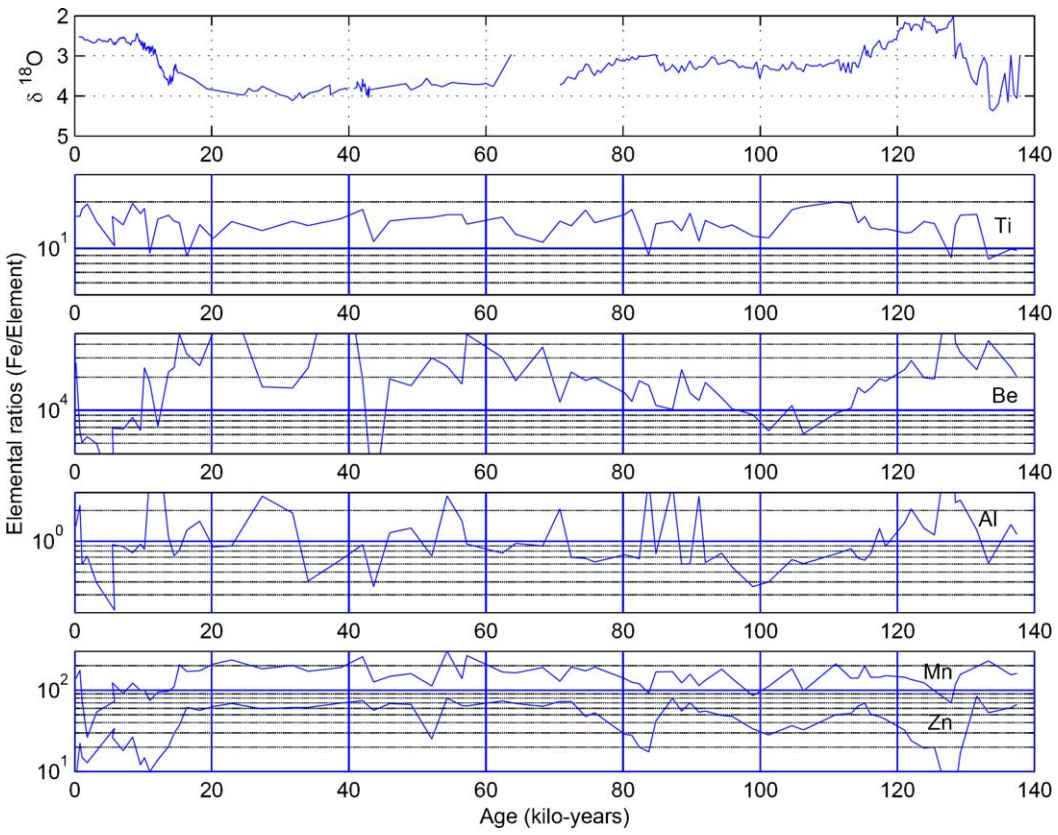

Fig. 9. The ratios of Fe/element concentrations for Ti, Be, Al, Mn and Zn in opal in the 140 kyr section in the core from site 1093, are plotted as a function of age of the sample, along with measured $\delta^{18}O$ values in the core.

deglaciations (e.g. Stage 6–5e) and stadial to interstadial transitions (e.g. Stage 5b–5a).

Despite their obvious temporal connection to the state of global climate–visual inspection of the Fe/Zn ratio, for example, suggests a clear 23,000 year cycle—these trends, like the scatter plots (Fig. 8), could be interpreted in a number of different ways. It is possible that the various assemblages of diatoms that prevailed over the course of an ice age cycle simply had different micronutrient requirements/uptake, and the sedimentary opal monitored the net result. In this case, the metal ratios do not necessarily speak to large scale patterns of net productivity. Alternatively, if one believes that the regional productivity was higher during the cold periods, then one could take the higher Fe/Zn or Fe/Mn ratios in the diatoms during ice ages to be a measure of increased biological drawdown of Zn and Mn. (As above, an additional inference in this case is that Fe must have been less important than the other essential micronutrients.) Still another possibility exists: if one believes that diatom productivity was maximized during deglaciation and early interglacial episodes, then the reduced Fe/Zn or Fe/Mn ratios at these times could be a sign of preferential uptake of iron during highest diatom growth rate—as is observed for the iron seeding analyses in the modern ocean (Coale et al., 2003). This explanation could also be consistent with the Be and Al evidence, which point to highest particle scavenging during the early deglaciation. This explanation is also consistent with the overall accumulation rate of opal in the sediments at the Antarctic Polar Front, which was highest during the deglaciations and early interglacial periods. However, this explanation goes in the opposite direction for invoking a Southern Ocean biological control on atmospheric CO_2 fluctuations, because atmospheric CO_2 increased significantly during each of the episodes of reduced opaline Fe/Zn or Fe/Mn.

While we believe that the balance of evidence favors the latter interpretation, we cannot as yet rule out the other possibilities. Given that these various interpretations for metal behavior are mutually incompatible, the significant remaining uncertainties emphasize the need for obtaining a true estimate of particle (and metal) flux from the surface waters through a full ice age cycle. Estimates of opal-derived metal flux to the sediment are possible with just the concentration data, but these estimates are not free of complications such as post-depositional mobilization and sediment focusing by bottom currents. On the other hand, we are optimistic that the combined measurement of trace metals and $^{26}Al/Al$ ratios in splits of the same opal material could yield a quantitative estimate of relative rates of productivity across intervals of different climate state.

6. Conclusions

The tests of marine organisms have long been used as archives for studying physical and chemical changes in the

oceans in the past. Our investigations of the concentrations of trace elements and of cosmogenic ^{10}Be and ^{26}Al in the three principal biogenic minerals: coral aragonite, foraminiferal calcite, and radiolarian opal led to the finding that 'opal' displays the largest distribution coefficient for the biologically and geochemically important elements: Be, Mg, Al, Ca, Ti, Mn, Fe and Zn. The concentration levels of several elements in opal are high enough (∼mg/g for Al, Ca, Fe, Mg and Ti and ∼μg/g for Be, Mn, Zn and Sr) that they can easily be measured accurately in mg quantities of opal using ICP-OES (Table 1). This contrasts with the typical concentrations of several trace elements in foraminifera and in corals at 1–100 ppb levels (Boyle, 1992; Dong et al., 2001). Because of the high enrichments of Be and Al, dissolved concentrations of cosmogenic nuclides, ^{10}Be and ^{26}Al concentrations are also relatively easy to measure in biogenic opal. The data presented here show that ^{10}Be can easily be measured in ∼100 mg opal, and ^{26}Al in ∼10 g opal (Table 2).

To make a preliminary study of the potentials of the marine opal, we have studied a 140 kyr long time series of concentrations of a suite of trace elements and cosmogenic nuclide, ^{10}Be in two sediment cores from the Southern Ocean diatomaceous ooze belt, near the present-day position of the Antarctic Polar Front. The observed consistent patterns in the temporal variations of trace element, and ^{10}Be and ^{26}Al, concentrations with δ^{18}O over a time range of 140 kyr clearly establish the important fact that the opaline frustules faithfully record their dissolved concentrations. Thus, with one sedimentary phase and in single sedimentary sections, we now have the potential to compare directly a proxy for aeolian input of micronutrients (e.g. Fe or Ti), with a proxy for production (e.g. ^{26}Al/Al ratios).

Our limited data lead to the following conclusions:

(1) The opaline frustules faithfully record the temporal variations of trace elements, Be, Al, Ti, Fe, Mn and Zn, and of cosmogenic nuclides ^{10}Be concentrations with δ^{18}O over a time range of 140 kyr dissolved concentrations. How far this time range can be extended depends on the degree of preservation of opaline matrix in the sediment.

(2) The aeolian dust fluxes to the ocean near the present-day position of the Antarctic Polar Front are highly variable during one glacial/interglacial cycle, leading to more than 20-fold increases in the dissolved concentrations of Fe and Ti. The net visible increases in the dissolved concentrations of bioreactive elements, Al, Mn and Zn are by an order of magnitude.

(3) In regions of high opal productivity, opal may be an important agent for removing dissolved concentrations of biologically important trace elements, Fe, Al, Mn and Zn from surface waters. If this suggestion is validated by further work, it suggests that future iron fertilization experiments must also consider corresponding additions of Al, Mn and Zn.

(4) There is possible evidence for the increase of biological productivity with increased aeolian fluxes (which we judge by increases in the dissolved concentrations of Fe and Ti). Fe and Ti co-vary strongly, and since Ti is not indicated to be an important element in influencing biological productivity, we conclude that except possibly for initial additions of small amounts to Fe to iron impoverished waters, further increase in Fe does not affect biological productivity. However, the various metal ratios change with climate in ways that suggest a range of possible interpretations of regional productivity.

(5) Higher aeolian fluxes in the sediment cores studied are associated with increased fluxes of ^{10}Be to the oceans, which are most probably due to the influx of surface dusts from Patagonia. Dust fluxes decrease the dissolved ^{10}Be/Be ratios in the oceans by about a factor of ∼3. Similar behavior is expected in the case of ^{26}Al, but the magnitude of change in the absolute concentrations and ratios are expected to be very different from those observed for ^{10}Be.

Pending settlement of the important questions above, namely the mechanisms by which opal includes trace elements in its structure, we can now proceed to use it as a veritable recorder of dissolved concentrations in surface waters.

Acknowledgments

We are deeply grateful to M. Hildebrand for very valuable discussions on mechanisms of trace element trapping in opaline frustules. This work was supported in part from NSF Grant OCE-0426424. One of us (D.L.) thanks Joan Eichen and late Myron Eichen for their invaluable support and encouragement throughout this research.

Associate editor: John Crusius

References

Barg, E., Lal, D., Southon, J.R., Caffee, M.W., Finkel, R.C., Pavich, M.J., 1997. Beryllium geochemistry in soils: evaluation of ^{10}Be/^{9}Be ratios in authigenic minerals as a basis for age models. *Chem. Geol.* **140**, 237–258.

Basile, I., Grousset, F.C., Ravel, M., Petit, J.R., Biscaye, P.E., Barkov, N.I., 1997. Patgonian origin of glacial dust deposited in East Antractica (Vostok and Dome C) during glacial stages 2, 4 and 6. *Earth Planet. Sci. Lett.* **146**, 573–589.

Bigg, G.R., Jickells, T.D., Liss, P.S., Osborn, T.J., 2003. The role of oceans in climate. *Int. J. Climatol.* **23**, 1127–1159.

Boyle, E.A., 1992. Cadmium and δ^{13}C paleochemical ocean distributions during the stage 2 glacial maximum. *Annu. Rev. Earth Palnet. Sci.* **20**, 245–287.

Brown, E.B., Measures, C.I., Edmond, J.M., Bourles, D.L., Raisbeck, G.M., Yiou, F., 1992. Continental inputs of beryllium to the oceans. *Earth Planet. Sci. Lett.* **114**, 101–111.

Charles, C.D., Froelich, P.N., Zibello, M.A., Mortlock, R.A., Morley, J.J., 1991. Biogenic opal in Southern Ocean sediments over the last

450,000 years: implications for surface water chemistry and circulation. *Paleoceanography* **6**, 697–728.

Chase, Z., Anderson, R., Fleisher, M., Kubik, P., 2003. Accumulation of biogenic and lithogenic material in the Pacific sector of the Southern Ocean during the past 40,000 years. *Deep Sea Res. Part II* **50**, 799–832.

Coale, K.H., Wang, X., Tanner, S.J., Johnson, K.S., 2003. Phytoplankton growth and biological response to iron and zinc addition in the Ross Sea and Antarctic Circumpolar current along 170° W. *Deep Sea Res. Part II* **50**, 635–653.

Criscenti, L.J., Sverjensky, D.A., 1999. The role of electrolyte anions (ClO_4, NO_3, and Cl^-) in divalent metal (M^{2+}) adsorption on oxide and hydroxide surfaces in salt solutions. *Am. J. Sci.* **299**, 828–899.

de Baar, H.J.W., de Jong, T.M., Bakker, D.C.E., Loscher, B.M., Veth, C., Bathmann, U., Smetacek, V., 1995. Importance of iron for plankton blooms and carbon dioxide drawdown in the Southern ocean. *Nature* **373**, 412–415.

Dixit, S., Van Cappellen, P., 2002. Surface chemistry and reactivity of biogenic silica. *Geochim. Cosmochim. Acta* **66**, 2559–2568.

Dong, W., Lal, D., Ransom, B., Berger, W., Caffee, M.W., 2001. Marine biogeochemistries of Be and Al: a study based on cosmogenic ^{10}Be, Be and Al in marine calcite, aragonite and opal. *Proc. Ind. Acad. Sci. (Earth and Planet. Sci.)* **11** (2), 95–102.

Elderfield, H., Rickaby, R.E.M., 2000. Oceanic Cd/P ratio and nutrient utilization in the glacial Southern Ocean. *Nature* **405**, 305–310.

Ellwood, M.J., Hunter, K.A., 1999. Determination of the Zn/Si ratio in diatom opal: a method for the separation cleaning and dissolution of diatoms. *Mar. Chem.* **66**, 149–160.

Ellwood, M.J., Hunter, K.A., 2000. Variations in the Zn/Si record over the last interglacial transition. *Paleoceanography* **15**, 506–514.

Ganeshram, R., Pedersen, T., 1998. Glacial–interglacial variability in upwelling and bioproductivity off NW Mexico: implications for Quaternary paleoclimate. *Paleoceanography* **13**, 634–645.

Gersonde, R., Abelmann, A., Brathauer, U., Becquey, S., Bianchi, C., Cortese, G., Grobe, H., Kuhn, G., Niebler, H.S., Segl, M., Sieger, R., Zielinski, U., Futterer, D.K., 2003. Last glacial sea surface temperatures and sea-ice extent in the Southern Ocean (Atlantic-Indian sector): A multiproxy approach. *Paleoceanography* **1** (3), 1061.

Hildebrand, M., Wetherbee, R., 2003. Components and control of silicification in diatoms. In: Mueller, W.E.G. (Ed.), *Progress in Molecular and Subcellular Biology, Silicon Biomineralization*, 3. Springer-Verlag, Heidelberg, pp. 11–57.

Hodell, D.A., Charles, C.D., Curtis, J.H., Mortyn, P.G., Ninnemann, U.S., Venz, K.A., 2002. Data report: oxygen isotope stratigraphy of ODP Leg 177 Sites 1088, 1089, 1090, 1093, and 1094, Proc. ODP, Sci. Results 177, Ocean Drilling Program, College Station, TX. <http://www-odp.tamu.edu/publications/177_SR/>.

Jouzel, J., Barkov, N.I., Barnola, J.M., Bender, M., Chappellaz, J., Genthon, C., Kotlyakov, V.M., Lipenkov, V., Lorius, C., Petit, J.R., Raynaud, D., Raisbeck, G., Ritz, C., Sowers, T., Stievenard, M., Yiou, F., Yiou, P., 1993. Extending the Vostok ice-core record of paleoclimate to the penultimate glacial period. *Nature* **364**, 407–412.

Kanfoush, S., Hodell, D.A., Charles, C.D., Guilderson, T.G., Mortyn, P.G., Ninnemann, U.S., 2000. Millennial scale instability of the Antarctic Ice Sheet during the last glaciation. *Science* **288**, 1815–1818.

Keigwin, L.D., Boyle, E.A., 1989. Late Quaternary paleochemistry of high-latitude surface waters. *Paleoclimatol. Paleogeog. Paleoecol.* **73**, 85–106.

Kröger, N., Deutzmann, R., Bergsdorf, C., Sumper, M., 2000. Species-specific polyamines from diatoms control silica morphology. *Proc. Natl. Acad. Sci. USA* **97**, 14133–14138.

Kröger, N., Deutzmann, R., Sumper, M., 1999. Polycationic peptides from diatom biosilica that direct silica nanosphere formation. *Science* **286**, 1129–1132.

Ku, T.L., Kusakabe, M., Measures, C.I., Southon, J.R., Gusimano, G., Vogel, J.S., Nelson, D.E., Nakaya, S., 1990. Beryllium isotope distribution in the western North Atlantic: a comparison to the Pacific. *Deep-Sea Res.* **37**, 795–808.

Ku, T.L., Wang, L., Luo, S., Southon, J.R., 1995. ^{26}Al in seawater and ^{26}Al/^{10}Be as a paleo-flux tracer. *Geophys. Res. Lett.* **22**, 2163–2166.

Kumar, N., Anderson, R.F., Mortlock, R.A., Froelich, P.N., Kubik, P., Dittrich-Hannen, B., Suter, M., 1995. Increased biological productivity and export production in the glacial Southern Ocean. *Nature* **362** (6415), 675–680.

Kusakabe, M., Ku, T.L., Southon, J.R., Vogel, J.S., Nelson, D.E., Measures, C.I., Nozaki, Y., 1987. Distribution of ^{10}Be and ^{9}Be in the Pacific Ocean. *Earth Planet. Sci. Lett.* **82**, 231–240.

Lal, D., 2002. Marine biogenic minerals hold clues about changes in ocean chemistry and climate: some important lessons learned from studies of stable and radioactive isotopes of Be and Al. *Sci. World J.* **2**, 1267–1272.

Lal, D., Peters, B., 1967. Cosmic ray produced radioactivity on the earth. In: Flugge, S. (Ed.), *Handbuch der Physik*, vol. 46. Springer-Verlag, Berlin, pp. 551–612.

Latimer, J.C., Flippelli, G.M., 2001. Terrigenous input and paleoproductivity in the Southern Ocean. *Paleoceanography* **16**, 627–643.

Li, C.-W, Chu, S., Lee, M., 1989. Characterizing the silicon deposition vesicle of diatoms. *Protoplasma* **151**, 158–163.

Martin, J.H., 1990. Glacial–interglacial CO_2 change: the iron hypothesis. *Paleoceanography* **5**, 1–13.

Martin, J.H., Gordon, R.M., Fitzwater, S.E., 1990. Iron in Antacrctic waters. *Nature* **345**, 156–158.

Martin, J.M., Knauer, G.A., 1973. The elemental composition of plankton. *Geochim. Cosmochim. Acta* **37**, 1639–1653.

Mason, B., 1966. *Principles of Geochemistry*, third ed. Wiley, New York, p. 329.

Mayewski, P.A., Meeker, L.D., Twickler, M.S., Whitlow, S.I., Yang, Q., Lyons, W.B., Prentice, M., 1997. Major features and forcing of high-latitude northern hemisphere atmospheric circulation using a 110,000-year-long glaciochemical series. *J. Geophys. Res.* **102**, 26345–26366.

Measures, C.I., Ku, T.L., Luo, S., Southon, J.R., Xu, X., Kusakabe, M., 1996. The distribution of ^{10}Be and ^{9}Be in the South Atlantic. *Deep Sea Res.* **43**, 987–1009.

Measures, C.S., Vink, S., 2001. Dissolved Fe in the upper water of the Pacific sector of the southern Ocean. *Deep Sea Res. II* **48**, 3913–3941.

Mortlock, R.A., Charles, C.D., Froelich, P.N., Zibello, M.A., Saltzman, J., Hays, J.D., Burckle, L.H., 1991. Evidence for lower productivity in the Antarctic Ocean during the last glaciation. *Nature* **351**, 220–222.

Mortyn, P.G., Charles, C.D., 2002. Southern Ocean upper water column over the last 140 kyr with emphasis on the glacial terminations. *Global Planet. Change* **34**, 241–252.

Mortyn, P.G, Charles, C.D., Ninnemann, U.S., Ludwig, K., Hodell, D.A., 2003. Deep sea sedimentary analogs to the Vostok Ice Core. *Geochem. Geophys. Geosyst.* **4**. Art. No. 8405.

Rea, D., 1994. The paleoclimatic record provided by eolian deposition in the deep sea: the geologic history of wind. *Rev. Geophys.* **32**, 159–195.

Ridgewell, A.J., 2003. Implications of the glacial CO_2 "iron hypothesis" for quaternary climatic change G^3. *Geochem. Geophys. Geosyst.* **4** (9), 1076. doi:10.1029/2003GC000563.

Riley, J.P., Chester, R., 1981. *Introduction to Marine Chemistry*. Academic Press, New York, p. 465.

Shemesh, A., Macko, S.A., Charles, C.D., Rau, G.H., 1993. Isotopic evidence for reduced productivity in the glacial Southern Ocean. *Science* **262**, 407–410.

Sigman, D., Boyle, E.A., 2000. Glacial/interglacial variations in atmospheric carbon dioxide. *Nature* **407**, 859–869.

Watson, A.J., Bakker, D.C.E., Ridgwell, A.J., Boyd, P.W., Law, C.S., 2000. Effect of iron supply on Southern Ocean CO_2 uptake and implications for glacial atmospheric CO_2. *Nature* **407**, 730–733.